A New Implicit Method for Surface Segmentation by Minimal Paths: Applications in 3D Medical Images

Roberto Ardon[1,2], Laurent D. Cohen[2], and Anthony Yezzi[3]

[1] MEDISYS-Philips France, 51, rue Carnot, 92156 Suresnes, France
[2] CEREMADE-Université Paris Dauphine,
Place du Marchal de Lattre de Tassigny, 75775 Paris Cedex 16, France
[3] Georgia Institute of Technology, Atlanta, GA, USA
roberto.ardon@philips.com, cohen@ceremade.dauphine.fr,
ayezzi@ece.gatech.edu

Abstract. We introduce a novel implicit approach for single object segmentation in 3D images. The boundary surface of this object is assumed to contain two known curves (the constraining curves), given by an expert. The aim of our method is to find this surface by exploiting as much as possible the information given in the supplied curves. As for active surfaces, we use a cost potential which penalizes image regions of low interest (most likely areas of low gradient or away from the surface to be extracted). In order to avoid local minima, we introduce a new partial differential equation and use its solution for segmentation. We show that the zero level set of this solution contains the constraining curves as well as a set of paths joining them. These paths globally minimize an energy which is defined from the cost potential. Our approach is in fact an elegant, implicit extension to surfaces of the minimal path framework already known for 2D image segmentation. As for this previous approach, and unlike other variational methods, our method is not prone to local minima traps of the energy. We present a fast implementation which has been successfully applied to 3D medical and synthetic images.

Keywords: Image segmentation, Active contours, Minimal Paths, Level Set method, Object Extraction, Stationary Transport Equation.

1 Introduction

Since their introduction by Kass et al. [15], deformable models have been extensively used to find single and multiple objects in 2D and 3D images. The common use of these models consists in introducing an initial object in the image and deforming it until it reaches a desired target. In most applications, the evolution of the object is chosen in order to most rapidly reduce an energy involving the image data, until a steady state is reached. One of the main drawbacks of this approach is that it suffers from local minima 'traps'. This is the case when the steady state, reached by the active object, does not correspond to the target but to another local minimum of the energy. An immediate consequence of this behavior is that the active object's initialization is a crucial step, since the final result depends strongly upon it. Since the publication of [15], much work has been done in order to free active models from the problem of local minima.

A. Rangarajan et al. (Eds.): EMMCVPR 2005, LNCS 3757, pp. 520–535, 2005.

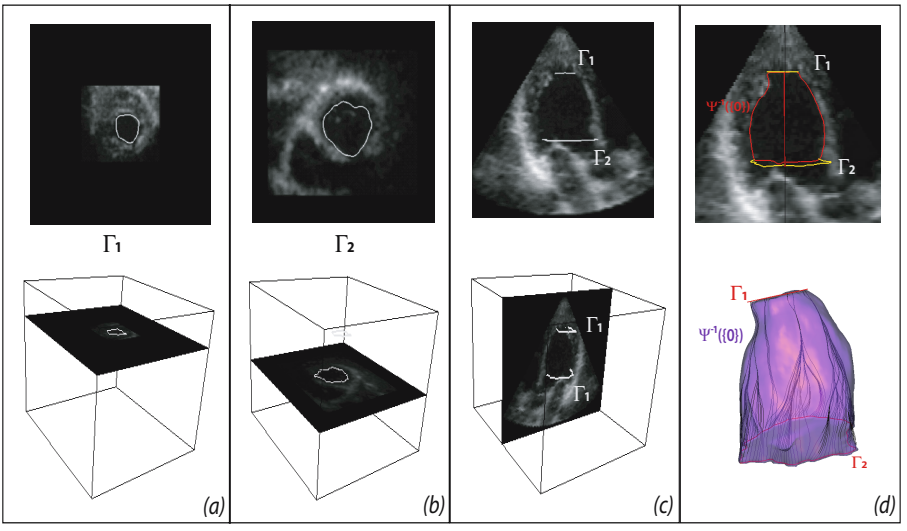

Fig. 1. 3D ultrasound volume of a left ventricle: (a) and (b) show the two parallel slices where the user given curves Γ_1 and Γ_2 are drawn. (c) shows a slice perpendicular to the curves in order to show their position with respect to the ventricle. Finally (d) shows the surface containing the constraint curves obtained with our approach. In the upper position we have shown the intersection of the zero level set of Ψ with a vertical plane. In the lower position we have traced some minimal paths between the two constraining curves and a 3D representation of the zero level set, the minimal paths are traced on this surface.

A balloon force was early proposed in [8] to make the model more active and to cope with the shrinking problem, but this force assumes a known direction in the evolution. The introduction of region dependent energies [9, 27, 19] and the use of shape priors approaches [26], contributed to create a more robust framework. In order to avoid local minima of the active contours, [10] proposed an approach to find a global minimum of the energy. However their approach cannot be extended to find the global minimum for an active surface in a 3D image.

In this work, we focus on a novel approach for 3D single object segmentation where the resulting surface globally minimizes a given energy. Our aim is to generate a surface that contains a couple of 'constraining' curves (Γ_1 and Γ_2) and which is also a segmentation of an object. Γ_1 and Γ_2 are supposed to be traced by an expert[1] on the surface to be segmented. Our approach is based on implicitly generating a surface that contains the set of paths globally minimizing an image energy and connecting Γ_1 and Γ_2. Moreover, the constraining curves are the only input for the initialization of our model. The paths linking Γ_1 and Γ_2 are globally minimal with respect to an energy of the form $\int_\Gamma \widetilde{\mathcal{P}}$. If the incremental cost $\widetilde{\mathcal{P}}$ is chosen to take lower values on the contours of the 3D image, in particular on the surface of the object to be extracted, global min-

[1] Notice that the expert may obtain these curves with a 2D active contour or interactive tool like with the minimal path approach in [13].

imal paths will help finding the boundary of the object (see section 2 and [10]). This fact has been exploited in previous work [2, 3], where a network of a *finite* number of minimal paths was computed between the two constraining curves and then extended, by means of interpolation, to a segmentation surface of the object.
Although this approach gave good results, particularly in ultrasound 3D images, the topology of the network was often problematic (paths tend to merge and only few points of Γ_1 are to be reached, see figure 1.d) considerably complicating the generation of the segmenting surface and, in the worst cases, leading to bad segmentations (figure 3.b).

Our work presented herein, although based on similar ideas, is much more than an implicit extension of the network approach. The surface generated by our algorithm is *completely* composed of *globally* minimal paths, and in particular, it contains all the minimal paths of the network introduced in [3]. Indeed, by solving a stationary transport equation of the form: $\nabla\Psi.\nabla U = 0$, where U is the action map (defined in section 3) and Ψ is the unknown, we show in section 4 that Ψ is such that: *any* minimal path between the constraining curves is contained in its zero level set $\Psi^{-1}(\{0\})$. We also prove that for almost any point of this level set, the minimal path between this point and Γ_1 is contained as well in $\Psi^{-1}(\{0\})$. This property is the key point explaining the good performance of our algorithm. In section 5 we give some results obtained by our method on synthetic and real data.

As an illustration of our problem, we give in figures 1.a, 1.b and 1.c an example of the user input to our algorithm. We perform the segmentation of a 3D ultrasound volume of the left ventricle. In figure 1.d we show the output of our method, which is the zero level set of function Ψ. We have also traced, for demonstration purposes, some minimal paths joining points of Γ_2 to Γ_1, which are clearly displayed on the segmented surface.

2 Minimal Paths in 2D Images

2.1 Active Contour Model

The first active contour model was introduced by Kass *et al.* in the seminal paper [15]. Their model, the well known 'snakes', consists in finding a curve $\mathcal{C}$ (parametrized on interval $[0, 1]$ and traced on the image) that minimizes the energy,

$$E_s(\mathcal{C}) = \int_0^1 \left\{ \alpha \left\| C'(x) \right\|^2 + \beta \left\| C''(x) \right\|^2 + \mathcal{P}(\mathcal{C}(x)) dx \right\}, \tag{1}$$

where α and β are positive constants. The minimization of the first two terms of E_s induces the curve $\mathcal{C}$ to have a relatively high regularity, while the minimization of the latter is intended to drive the curve toward significant edges of the image. In fact, Finding a curve that minimizes energy E is not a simple task; this functional is defined on the infinitely dimensioned space of regular curves and, generally, it is non-convex. The potential function $\mathcal{P}$ usually represents an edge detector that has lower values along edges. A common choice for this function is $\mathcal{P} = (1 + |\nabla I|^2)^{-1}$, if I is the image. Finding a curve that minimizes the energy E_s is not a simple task; this functional is defined on an infinite dimensional space and, generally, it is non-convex. The usual

approach is based on finding a local minimum of E_{snake} by evolving an initial curve $\mathcal{C}_0$ under the time dependent equation: $\frac{\partial \mathcal{C}(x,t)}{\partial t} - \alpha \frac{\partial^2 \mathcal{C}(x,t)}{\partial x^2} + \beta \frac{\partial^4 \mathcal{C}(x,t)}{\partial x^4} = -\nabla \mathcal{P}(\mathcal{C})$, with $\mathcal{C}(\cdot, 0) = \mathcal{C}_0$. By this approach, the final curve $\mathcal{C}$ is strongly dependent on the initialization $\mathcal{C}_0$. Since the method was originally intended to interactively segment a single object in the image, this behavior is rather natural. Nonetheless, if $\mathcal{C}_0$ is too far from the object to extract, the evolving curve can be trapped in another local minimum, thus giving an unsatisfactory result.

2.2 Active Contours and Minimal Paths

In order to obtain global minimization in the active contours framework, Cohen and Kimmel [10] simplified the energy by choosing $\beta = 0$ in the expression (1) of E_s. Additionally, they propose to use arclength parameterization (here noted s). Thus, they look for the curve minimizing energy

$$E(\mathcal{C}) = \int_0^L \left\{ \alpha + \mathcal{P}\big(\mathcal{C}(s)\big) \right\} ds \tag{2}$$

where L is the length of curve $\mathcal{C}$ and s its arclength parameterization (in the rest of this paper we shall note $\widetilde{\mathcal{P}} = \alpha + \mathcal{P}$). Even though this is the same energy proposed by Caselles *et al.*[6] and Yezzi *et al.* [24], used in the well-known geodesic active contour model, Cohen and Kimmel choose a completely different approach for the minimization of E. Instead of using an evolution equation as in [6, 15, 24], they exploit a method capable of building a curve between two points (p_1 and p_2) which is the global minimum of E among all the curves joining these points. This minimum is called a minimal path. Their approach is based on the fact that a minimal path between p_2 and p_1 can be obtained by 'back propagation', solving : $\frac{d\mathcal{C}}{dx}(x) = -\nabla U_{p_1}\big(\mathcal{C}(x)\big)$ with $\mathcal{C}(0) = p_2$. Where the real function U_{p_1}, called the minimal action map, is defined at each point q of the image domain by: $U_{p_1}(q) = \inf \left\{ \int_0^L \widetilde{\mathcal{P}}\big(C(s)\big) ds \right\}$. Where the inf is taken among all curves such that $\mathcal{C}(0) = p_1$ and $\mathcal{C}(L) = q$. In order to compute U_{p_1}, Cohen and Kimmel [10] use the fact (a proof of this fact can be found in [5]) that this map is solution to the well known Eikonal equation :

$$\|\nabla U_{p_1}\| = \widetilde{\mathcal{P}} \text{ and } U_{p_1}(p_1) = 0. \tag{3}$$

This equation is numerically solved by Cohen and Kimmel using the 'Fast marching' algorithm in order to compute a minimal path ([10]).

3 From Global Minimal Paths to 3D Surface Extraction

The method introduced in [10] can easily be extended for the construction of minimal paths between two points in a 3D image [12]. In that case, the formalism given in the previous section is unchanged, except for the fact that the functions $\widetilde{\mathcal{P}}, U_{p_1}$ are defined (and $\mathcal{C}$ takes its values) on a 3D domain. The authors of [12] used it to find centerlines in 3D tubular structures. As in the previous section, the cost function $\widetilde{\mathcal{P}}$ is supposed to

have lower values on a surface to be extracted from the 3D image. Before reviewing ideas in [2, 3], where the minimal path framework was extended to the extraction of surfaces between two given curves Γ_1 and Γ_2, we give for comparison purposes a brief description of the (now classical) geodesic active surface approach.

3.1 Background on Active Surfaces

The active surface model, introduced in [7], is a variational approach for the segmentation of objects in 3D images. In the same spirit as geodesic active contours, it is based on finding a surface which minimizes an energy of the form:

$$E_S(S) = \int_O \mathcal{P}(S) \left\| \frac{\partial S}{\partial u} \wedge \frac{\partial S}{\partial v} \right\| dudv, \tag{4}$$

where (u, v) are the parameters of S, defined on the open set $O \subset \mathbb{R}^2$. The most common procedure for finding a local minimum of this energy is to deform, until convergence, an initial surface S_0, according to the evolution equation:

$$\frac{\partial S}{\partial t} = \mathcal{P} H N_S - (\nabla \mathcal{P}.N_S)\, N_S \;\text{ with }\; S(\cdot,\cdot,0) = S_0, \tag{5}$$

H being the mean curvature of S and N_S its normal. This implies that the final surface is the local minimum of E_S which is "closest" to S_0. As with geodesic active contours, this method lacks robustness with respect to S_0. In [2] a method was suggested, based on minimal paths, that provided this model with a convenient initialization. This was done by incorporating the information given by the user through the two constraining curves, Γ_1, Γ_2. We give a description of this approach in the next section since our algorithm, further proposed, elaborates on ideas that are related.

3.2 Minimal Path Set Between Two Curves

Active surfaces are usually initialized with simple geometric structures like ellipsoids or cylinders which do not always lead to a good segmentation after evolution to a steady state. Here, instead, the user is asked to introduce into the 3D image a couple of curves (not necessarily planar) drawn on the surface to be extracted. These curves, Γ_1 and Γ_2, are exploited as the initialization of the model and as incorporated user information. The approach is based on considering a network of paths that globally minimizes an energy associated to the image. This network is used to generate a surface that contains the constraining curves and which provides a segmentation of the object lying between them.

We say that a curve $\gamma^q_{\Gamma_1}$ is a path between a point q and curve Γ_1 if $\gamma^q_{\Gamma_1}(0) = q$ and $\gamma^q_{\Gamma_1}(L) \in \Gamma_1$. A path network $\mathcal{N}^{\Gamma_2}_{\Gamma_1}$, between the points of Γ_2 and curve Γ_1, is the set

$$\mathcal{N}^{\Gamma_2}_{\Gamma_1} = \left\{ \gamma^q_{\Gamma_1} \right\}_{q \in \Gamma_2},$$

where it is supposed that every point q of Γ_2 is visited only once. Using the geodesic energy of each path composing the network, we define the following energy on the set of all possibles networks:

$$E_{Net}\left(\mathcal{N}_{\Gamma_1}^{\Gamma_2}\right) = \int_{q\in\Gamma_2}\int_0^{L(q)} \widetilde{\mathcal{P}}\left(\gamma_q^{\Gamma_1}(s)\right) dsdq. \tag{6}$$

Since the potential function $\widetilde{\mathcal{P}}$ is positive, the minimization of E_{Net} can be obtained by finding every globally minimal path between the points of Γ_2 and curve Γ_1. Moreover, these minimal paths are easily found. Indeed, similar to section 2.2, the minimal path between Γ_1 and a point q (further noted $\mathcal{C}_{\Gamma_1}^q$), with respect to the energy E (defined by (2)), is solution of the ordinary differential equation:

$$\frac{d\mathcal{C}_{\Gamma_1}^q}{dx}(x) = -\nabla U_{\Gamma_1}\left(\mathcal{C}_{\Gamma_1}^q(x)\right) \text{ with } \mathcal{C}_{\Gamma_1}^q(0) = q. \tag{7}$$

U_{Γ_1} is the action map defined on each point $q \in \Omega$ by :

$$U_{\Gamma_1}(q) = \inf\left\{\int_0^L \widetilde{\mathcal{P}}(\mathcal{C}(s))ds\right\},$$

where the inf is taken among all curves such that $C(0) = q$ and $\mathcal{C}(L) \in \Gamma_1$. Furthermore, it follows that $U_{\Gamma_1}(q) = \inf_{p\in\Gamma_1}\{U_p(q)\}$. This implies, as a consequence of relation (3), that U_{Γ_1} is also a solution to the Eikonal equation but with a different initial condition :

$$\|\nabla U_{\Gamma_1}\| = \widetilde{\mathcal{P}}, \text{ and } \forall p \in \Gamma_1, U_{\Gamma_1}(p) = 0. \tag{8}$$

By solving equation (7), using each point of Γ_2 as part of the initial condition, we globally minimize the energy E_{Net}, producing the minimal energy network:

$$\mathcal{S}_{\Gamma_1}^{\Gamma_2} = \bigcup_{q\in\Gamma_2}\left\{\mathcal{C}_{\Gamma_1}^q\right\}.$$

The minimal network is thus the set of all solutions of the ordinary differential equation (7) when varying its initial condition along Γ_2. Up to a reparameterization, assume every minimal path (respectively curve Γ_2) is parameterized on an interval J (respectively I). $\mathcal{S}_{\Gamma_1}^{\Gamma_2}$ can then be considered as a mapping (since minimal paths cannot cross without merging) from $I \times J$ to Ω, such that for all pair $(u, v) \in I \times J$ $\mathcal{S}_{\Gamma_1}^{\Gamma_2}(u, v) = \mathcal{C}_{\Gamma_1}^{\Gamma_2(u)}(v)$. Using this map for segmentation follows the same intuition as in [2, 3], where the hypothesis is made that each path of $\mathcal{S}_{\Gamma_1}^{\Gamma_2}$ is within a small distance from the surface to extract. Unfortunately, as can be understood from [18], in the general case the map $\mathcal{S}_{\Gamma_1}^{\Gamma_2}(\cdot,\cdot)$ lacks the fundamental property of continuity. For that reason, it is insufficient for segmentation. In order to cope with this difficulty, *Ardon* and *Cohen* [2, 3], proposed two different solutions :

– An analytical interpolation method was used to generate a surface from a finite number of paths belonging to $\mathcal{S}_{\Gamma_1}^{\Gamma_2}$. This approach gave satisfactory segmentation results only in very particular cases (the topology of the surface being such that the gaps created by the discontinuities uncover relatively small areas of the surface), and was thus preferred as an initialization of other active object methods [2].

– A different network was generated by solving a projected version of the ordinary differential equation (7) [3]. The projection was made on planes whose definition depended on Γ_1 and Γ_2. Even though satisfactory results were obtained in medical images under some restrictions applied to the two constraining curves (they should neither intersect nor be open), with this approach the network is no longer minimal for energy E_{Net}. Furthermore, paths can cross without merging thus no mapping can be defined. Last but not least, this approach can only extract surfaces of objects whose topology is cylindrical.

In order to solve the problems mentioned above, we introduce in the next section a novel approach for the generation of a surface using the minimal path network. This surface shall be defined as the zero level set of a function Ψ which solves a certain transport equation.

4 Implicit Definition of a Surface Containing the Minimal Paths Set

In order to simplify our description, Γ_1 and Γ_2 are assumed to be two non-intersecting planar, closed curves. We look for a real function Ψ, defined on the image domain Ω, such that $\mathcal{S}_{\Gamma_1}^{\Gamma_2}$ is contained in its zero level set (further noted $\Psi^{-1}(\{0\})$). Having no *a priori* knowledge on the properties Ψ should satisfy, we shall suppose that Ψ is continuously differentiable and we first look for a necessary condition based on our knowledge of the minimal path network. Further, this condition is exploited to formulate a sufficient condition and finally give a consistent description of function Ψ.

4.1 Searching for an Implicit Function

As in section 3.2, we denote by $\mathcal{C}_{\Gamma_1}^q$ a minimal path from a point $q \in \Omega$ to curve Γ_1, and we suppose that J is its parameterization interval. The minimal paths set $\mathcal{S}_{\Gamma_1}^{\Gamma_2}$ can also be considered as a subset of Ω, $p \in \mathcal{S}_{\Gamma_1}^{\Gamma_2}$ means that p is a point belonging to a minimal path. Let us first assume that a continuously differentiable function Ψ, defined in Ω is such that $\mathcal{S}_{\Gamma_1}^{\Gamma_2} \subset \Psi^{-1}(\{0\})$. This means that for all minimal path $\mathcal{C}_{\Gamma_1}^q$ we have $\forall x \in J, \Psi\big(\mathcal{C}_{\Gamma_1}^q(x)\big) = 0$. From the derivative with respect to x of this relation we obtain

$$\forall x \in J, \nabla\Psi\big(\mathcal{C}_{\Gamma_1}^q(x)\big).\frac{d\mathcal{C}_{\Gamma_1}^q}{dx}(x) = 0.$$

Using relation (7) we deduce the following proposition:

Proposition 4.11 (Necessary condition). *For any real differential function Ψ defined on Ω such that $\mathcal{S}_{\Gamma_1}^{\Gamma_2} \subset \Psi^{-1}(\{0\})$, we have for every point p of $\mathcal{S}_{\Gamma_1}^{\Gamma_2}$:*

$$\nabla\Psi(p).\nabla U_{\Gamma_1}(p) = 0. \tag{9}$$

The perpendicularity of the two gradient vector fields is only necessary on the points of the minimal path network. Hardening this condition and demanding that Ψ satisfies relation (9) everywhere in Ω, should lead to a sufficient relation for the minimal paths to be contained in $\Psi^{-1}(\{0\})$.

Proposition 4.12 (Sufficient condition). *If Ψ is a C^1 function satisfying :*

$$\begin{cases} (C_1)\ \forall p \in \Omega, \nabla\Psi(p).\nabla U_{\Gamma_1}(p) = 0 \\ (C_2) \qquad\qquad \forall q \in \Gamma_2, \Psi(q) = 0 \end{cases} \quad \textit{then } \mathcal{S}_{\Gamma_1}^{\Gamma_2} \subset \Psi^{-1}(\{0\}).$$

Proof: for every point $q \in \Gamma_2$, the values taken by function Ψ along the minimal path $C_{\Gamma_1}^q$ are given by function $f_q = \Psi \circ \mathcal{C}_{\Gamma_1}^q$. The derivative of f_q, for all $x \in J$, gives:

$$\begin{aligned} \frac{df_q}{dx}(x) &= \nabla\Psi\big(\mathcal{C}_{\Gamma_1}^q(x)\big).\frac{d\mathcal{C}_{\Gamma_1}^q}{dx}(x) \\ &\underbrace{=}_{\text{from (7)}} -\nabla\Psi\big(\mathcal{C}_{\Gamma_1}^q(x)\big).\nabla U_{\Gamma_1}\big(\mathcal{C}_{\Gamma_1}^q(x)\big) \underbrace{=}_{\text{from } (C_1)} 0. \end{aligned}$$

Thus, function f_q is constant on J. Furthermore, recall that $C_{\Gamma_1}^q(0) = q$ and $q \in \Gamma_2$. Condition (C_2) establishes then that $f_q(0) = 0$ and finally that f_q is zero on J, which means that Ψ is zero along any minimal path.
In the previous reasoning, the fact that point q belongs to Γ_2 is not relevant for establishing that f_q is a constant function. As a matter of fact, for every point $p \in \Psi^{-1}(\{0\})$ (not necessary on Γ_2), along the minimal path between this point and curve Γ_1, function Ψ also has zero values (since $f_p = 0$). This means that the set $\Psi^{-1}(\{0\})$ contains a set of minimal paths which is much larger than $\mathcal{S}_{\Gamma_1}^{\Gamma_2}$. More interestingly, we have:

Proposition 4.13 ($\Psi^{-1}(\{0\})$ structure). *If Ψ satisfies the same conditions as in property 4.12, then for all $p \in \Psi^{-1}(\{0\})$, the minimal path $\mathcal{C}_{\Gamma_1}^p$ joining p to Γ_1 satisfies $\mathcal{C}_{\Gamma_1}^p \subset \Psi^{-1}(\{0\})$.*

This establishes that the zero level set of the function Ψ is in fact a set of minimal paths joining Γ_1. Being minimal with respect to the geodesic energy E (see section 2.2), these paths tend to be traced on the object to extract (as Γ_1 and Γ_2). This explains the better results, compared to [3], obtained with our method, more information is injected into the model. A good example is given in figure 3, which demonstrates, on a synthetic image, how this approach gives good results where clearly $\mathcal{S}_{\Gamma_1}^{\Gamma_2}$ is insufficient for segmentation. In the next sections we outline two different manners to derive advantages from these propositions. The first one, is a direct implementation of the transport problem, the second is a combination with other active object approaches such as the active surface model.

4.2 Segmenting with the Transport Equation

We further denote by Π_1, Π_2 the intersection of the planes containing Γ_1 and Γ_2 with the image domain. The functions d_1, d_2 are the signed distance functions to these curves, positive in their interior and defined on Π_1 and Π_2 respectively. Notice that at each point $q \in \Gamma_2, d_2(q) = 0$.

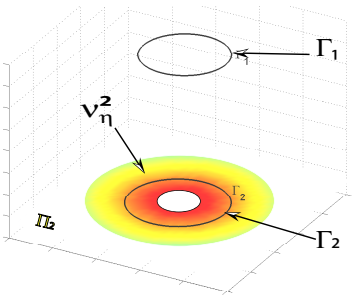

Fig. 2. Boundary conditions for the transport problem

Consider now the closed set

$$\mathcal{V}_\eta^2 = \{p \in \Pi_2 \text{ such that } |d_2(p)| \leqslant \eta\},$$

where η is a real positive value (see figure 2). Inspired by proposition 4.12, we consider the open set $\mathcal{O} = \text{int}(\Omega) - \mathcal{V}_\eta^2$, where $\text{int}(\Omega)$ is the interior of the image domain, and search for Ψ as the solution to the Cauchy problem defined on Ω:

$$\begin{cases} \nabla\Psi(p).\nabla U_{\Gamma_1}(p) = 0 & \text{if } p \in \mathcal{O}, \\ \Psi(p) = d_2(p) & \text{if } p \in \mathcal{V}_\eta^2, \\ \Psi(p) = \min\limits_{p \in \Pi_2} \big(d_2(p)\big) & \text{if } p \in \delta\Omega. \end{cases} \tag{10}$$

$\delta\Omega$ is the boundary of the image domain Ω. Problem (10) is known as a stationary transport problem: its solution Ψ, being constant along minimal path, "transports" the values taken along the boundary $\mathcal{V}_\eta^2 \cup \delta\Omega$.

The transport problem (10) has been studied from a theoretical point of view (see for example [1] and references within), and results of existence and uniqueness have been given by Bouchut *et. al.* in [4] and L. Ambrosio in [1]. It is beyond the scope of this paper to present the theoretical details. As a matter of fact, numerical approaches (see section 4.4) that take in consideration the presence of possible discontinuities of the function Ψ were proposed before a theoretical framework was established. Section 4.4 describes a fast algorithm for solving this problem.

4.3 A New Force for Active Models

Another approach for solving the stationary transport problem is to look for the steady state of the time dependent equation: $\frac{\partial\Psi}{\partial t} = \nabla\Psi.\nabla U_{\Gamma_1}$. In the level set formulation of the active surface model (see section 3.1 and [7]), the time dependent equation to solve, in the Level Set formulation [21], is: $\frac{\partial\Phi}{\partial t} = \nabla\Phi.\nabla\widetilde{\mathcal{P}} + \widetilde{\mathcal{P}}\,\|\nabla\Phi\|\,\text{div}\left(\frac{\nabla\Phi}{\|\nabla\Phi\|}\right)$. The first term of the right hand side is a transport term that drives the level sets of Φ to the minima of $\widetilde{\mathcal{P}}$. The second induces a regularization of Φ, which is dominant in areas where $\widetilde{\mathcal{P}}$ is strong. It is thus natural to introduce the same regularization in our problem and solve

$$\frac{\partial\Psi}{\partial t} = \nabla\Psi.\nabla U_{\Gamma_1} + U_{\Gamma_1}\,\|\nabla\Psi\|\,\text{div}\left(\frac{\nabla\Psi}{\|\nabla\Psi\|}\right)$$

(because Ψ would minimize a geodesic energy where U_{Γ_1} plays the role of the potential). A small inconvenience arises near Γ_2 since U_{Γ_1} can be strong in that area, thereby enforcing too much smoothing. The final surface may not strictly contain the constraining curves.

A different option is to consider our transport term as a new external force that drives the model toward the minimal path network, thus introducing the information given by

the user through the constraining curves as well as the global information contained in the function U. The dynamic equation to solve is then of the form:

$$\frac{\partial \Psi}{\partial t} = \nabla\Psi.\nabla\widetilde{\mathcal{P}} + \widetilde{\mathcal{P}}\,\|\nabla\Psi\|\,\mathrm{div}\left(\frac{\nabla\Psi}{\|\nabla\Psi\|}\right) + \underbrace{\nabla\Psi.\frac{\nabla U_{\Gamma_1}}{\|\nabla U_{\Gamma_1}\|}}_{\text{normalized force}}.$$

We have here considered the active surface model but our 'minimal path' force can be added to other active surface models as well. Of course, unlike the direct segmentation with the transport equation, while this new force contributes to avoiding unwanted local minima of the energy, it does not ensure the reaching of a global minimum. In what follows we will concentrate on the numerical solution to the transport problem and will leave further development of the method presented in this section to future papers.

4.4 Implementation of the Transport Problem

We now describe an efficient algorithm for the numerical implementation of the transport problem (10). Unlike [3], minimal paths are not to be computed directly in this implicit approach. We only numerically calculate solutions to the Eikonal and to the stationary transport equations.

To numerically solve the Eikonal equation (8) classic finite difference schemes tend to be unstable. Generally it is preferable to use consistent algorithms using *upwind* differences (derivative approximations are chosen looking in the direction from which the information is flowing) as fast marching [23, 20] or fast sweeping [14]. Numerical complexity of $O(N)$ (N being the number of grid points) can then be achieved and only one grid pass is needed to obtain a first order approximation of the solution U_{Γ_1}.

The stationary transport equation, as with most first order partial differential equations whose characteristics intersect, is difficult to solve numerically. In fact, in the general case ($\widetilde{\mathcal{P}}$ is supposed to be a bounded and continuous function), there is no classical solution defined in all Ω, and the weak solution Ψ can present discontinuities. Many implementations of the transport equation in its non-static expression have been proposed in the modeling of geophysical phenomena. In 1964, Lax and Wendorff proposed in [16] a scheme using centered finite differences for the approximation of derivatives. Then, in 1968, Crowley suggested in [11] a scheme that achieved second order precision in time and space, and which inspired other numerous publications. In particular, a generalization to multiple dimensions was proposed by Smolarkiewicz in [22]. These are only some early publications from a long list of papers treating this topic. Here we will concentrate on a first order, fast algorithm which is less constrained since only the zero level set of the solution matters in our approach.

In order to simplify notation, the symbol V shall be used to refer to the gradient ∇U_{Γ_1}. One of the first numerical approaches for solving the transport equation proposes a first order approximation of the gradient $\nabla\Psi$ that follows the direction in which information propagates. This discretization is the *upwind* approach and

consists in choosing the approximation of $\frac{\partial \Psi}{\partial \alpha}$ following the sign of the components V_α (where $\alpha = x, y$ ou z) of V. Recently, A. Yezzi and J. L. Prince used this scheme in [25] for the numerical solution of equation $\nabla \Psi . T = 1$ (where T was a known vector field). Lastly, although this scheme is of relatively low precision and dissipative [17], it gives satisfactory results in our experiments with an acceptable convergence speed.

If $\Psi^{i,j,k}$ is the value of the numerical approximation of Ψ at point $[i; j; k]$ of the discrete square grid, we shall denote the left and right approximations of the partial derivatives by:

$$D^{-x}\Psi = \frac{\Psi^{i,j,k} - \Psi^{i-1,j,k}}{h}, \; D^{+x}\Psi = \frac{\Psi^{i+1,j,k} - \Psi^{i,j,k}}{h}$$

(similarly in the y and z directions) where h is the discretization step, identical in all three spatial directions. Our scheme for solving the stationary transport problem $V.\nabla\Psi = 0$ is then

$$V_x^{i,j,k}.\left(D^{-x}\Psi^{i,j,k} \text{ or } D^{+x}\Psi^{i,j,k}\right) + V_y^{i,j,k}.\left(D^{-y}\Psi^{i,j,k} \text{ or } D^{+y}\Psi^{i,j,k}\right) + V_z^{i,j,k}.\left(D^{-z}\Psi^{i,j,k} \text{ or } D^{+z}\Psi^{i,j,k}\right) = 0.$$

In our problem, the direction in which information propagates is given by the vector $-V$. Therefore, denoting by H the heaviside function defined by $H(x) = \begin{cases} 1, \text{ if } x \geqslant 0 \\ 0, \text{ else.} \end{cases}$,

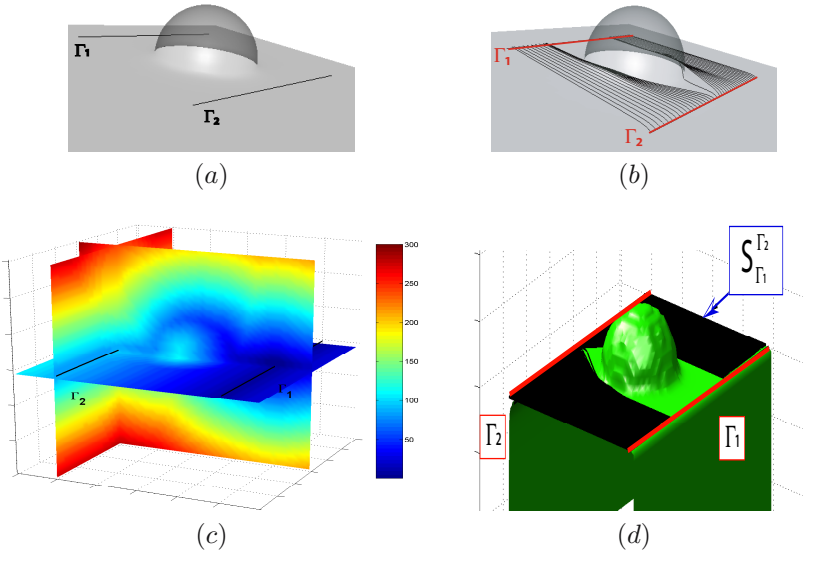

Fig. 3. (a) represents a half-sphere blended with a plane (transparent visualization) and Γ_1 and Γ_2 (black segments). (b) shows some minimal paths of $\mathcal{S}_{\Gamma_1}^{\Gamma_2}$ taking a short cut around the sphere. (c) shows the values taken by Ψ on three perpendicular planes. (d) shows the superposition of $\Psi^{-1}(0)$ and the set $\mathcal{S}_{\Gamma_1}^{\Gamma_2}$ (see please the electronic color version).

the *upwind* approximation is:

$$\begin{array}{l} V_x^{i,j,k}.\big(D^{-x}\Psi^{i,j,k}H(-V_x^{i,j,k}) + D^{+x}\Psi^{i,j,k}H(V_x^{i,j,k})\big)+ \\ V_y^{i,j,k}.\big(D^{-y}\Psi^{i,j,k}H(-V_y^{i,j,k}) + D^{+y}\Psi^{i,j,k}H(V_y^{i,j,k})\big)+ \\ V_z^{i,j,k}.\big(D^{-z}\Psi^{i,j,k}H(-V_z^{i,j,k}) + D^{+z}\Psi^{i,j,k}H(V_z^{i,j,k})\big)= 0. \end{array}$$

Then, if $I = (i+1)$ if $V_x > 0$, $i-1$ otherwise, and similarly for J and K, we have

$$\begin{array}{c} \big|V_x^{i,j,k}\big|\big[\Psi^{I,j,k} - \Psi^{i,j,k}\big]+\big|V_y^{i,j,k}\big|\big[\Psi^{i,J,k} - \Psi^{i,j,k}\big] \\ +\big|V_z^{i,j,k}\big|\big[\Psi^{i,j,K} - \Psi^{i,j,k}\big]= 0, \end{array}$$

which, by grouping terms with $\Psi^{i,j,k}$, finally leads to the update expression of our algorithm:

$$\Psi^{i,j,k} = \frac{|V_x^{i,j,k}|\Psi^{I,j,k} + |V_y^{i,j,k}|\Psi^{i,J,k} + |V_z^{i,j,k}|\Psi^{i,j,K}}{|V_x^{i,j,k}| + |V_y^{i,j,k}| + |V_z^{i,j,k}|}. \tag{11}$$

This equality can be exploited, as presented in [25], in a fast marching type scheme that achieves a first order approximation of the solution to our problem in only one grid

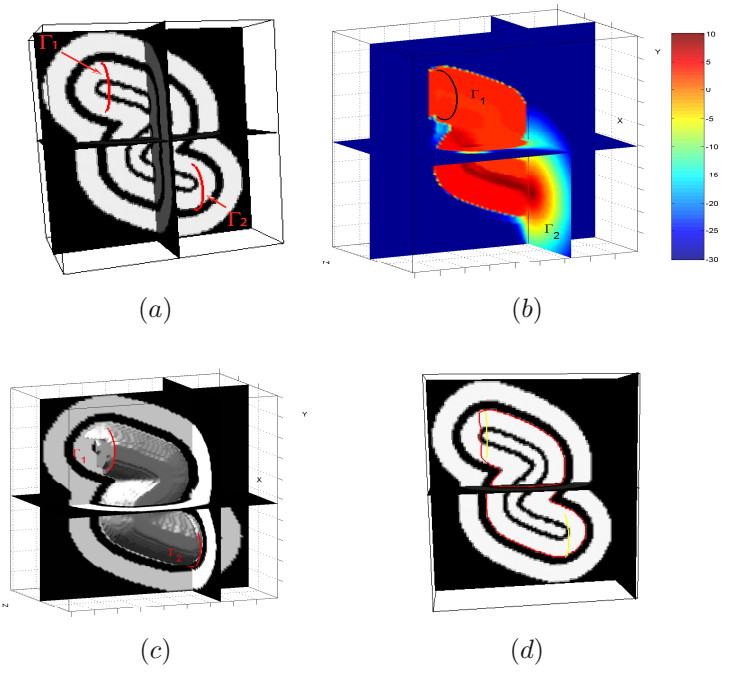

Fig. 4. (a) shows the intersection of a plain with a binary image where three 'S' shaped tubes are one inside the other, Γ_1 and Γ_2 are shown in red. (b) shows the values taken by Ψ on three perpendicular planes (see please the electronic color version). (c) shows the superposition of $\Psi^{-1}(0)$ and the original image and (d) the intersection of this surface with a plane of the image.

pass and with a $N \log(N)$ complexity. In the end, our algorithm consists in solving the Eikonal equation first, then the transport equation by means of the same implementation. We thus can achieve very rapid computing times. In the next section we give some results.

5 Applications

We apply our method to some synthetic and real 3D images. In all our examples we used a potential of the form: $\widetilde{\mathcal{P}} = \alpha.h(|\nabla I_\sigma|) + (1-\alpha).h_{gap}(\Delta I_\sigma)$, where h and h_{gap} are two functions bounded between 0 and 1 and where I_σ is the convolution of the given image with a Gaussian kernel of variance σ. Typically, $h(x) = \frac{1}{1+x^2/\lambda^2}$, where λ is a user defined contrast factor that can be computed as an average gradient value, and h_{gap} is chosen to be a zero crossing detector.

Figure 3 represents a sphere blended with a plane. This surface is to be extracted between two curves which are parallel lines (see figure 3.a). This configuration does not exactly satisfy the hypothesis taken in section 3 (we are not dealing with closed curves) but the extension is straightforward (the boundary conditions have to be slightly modified). The set of minimal paths $\mathcal{S}_{\Gamma_1}^{\Gamma_2}$ is unable to provide enough information for

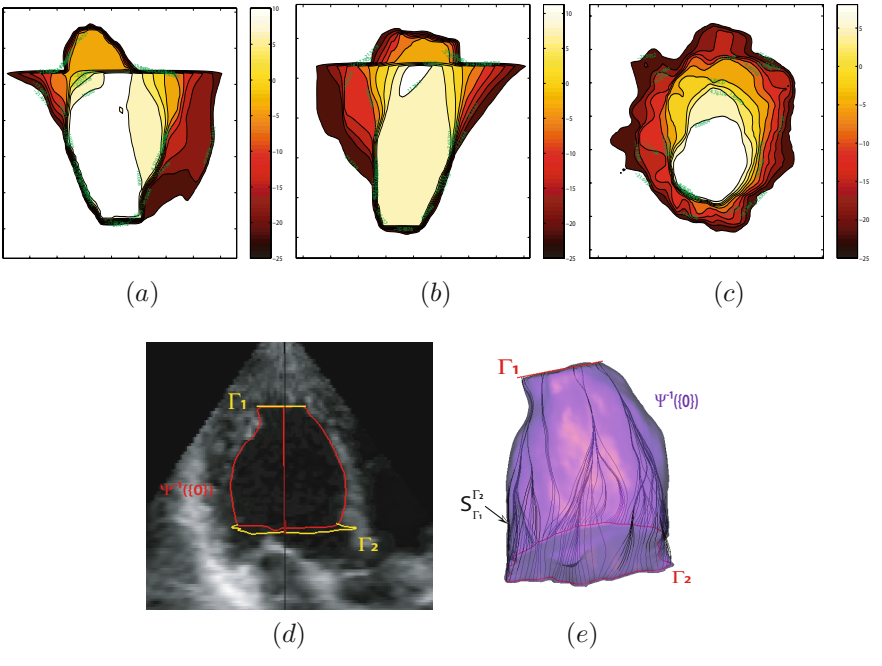

Fig. 5. Left ventricle segmentation : (a),(b) and (c) display some level sets of our solution Ψ on three orthogonal planes. (d) shows the intersection of the zero level set of Ψ with a slice of the image and (e) shows a volume representation of $\Psi^{-1}(\{0\})$ (see please the electronic color version).

the extraction of the surface, since no minimal path 'climbs' on the sphere surface. Nonetheless, the zero level set of the corresponding Ψ function reconstructs perfectly the surface. Our implicit method recovers more information than the minimal paths and we obtain the complete surface.

Figure 4 illustrates with a synthetic binary volume the behavior of our algorithm when various local minima of energy E_S (4) are present. In this volume three 'S' shaped tubes are displayed one inside the other. The constraining curves are traced on the second tube, without the information they bring, segmenting this tube is a hard task.

In figure 5 we show the extraction of the surface of the left ventricle from the 3D ultrasound image shown in figure 1. For this ultrasound image of size $256 \times 256 \times$

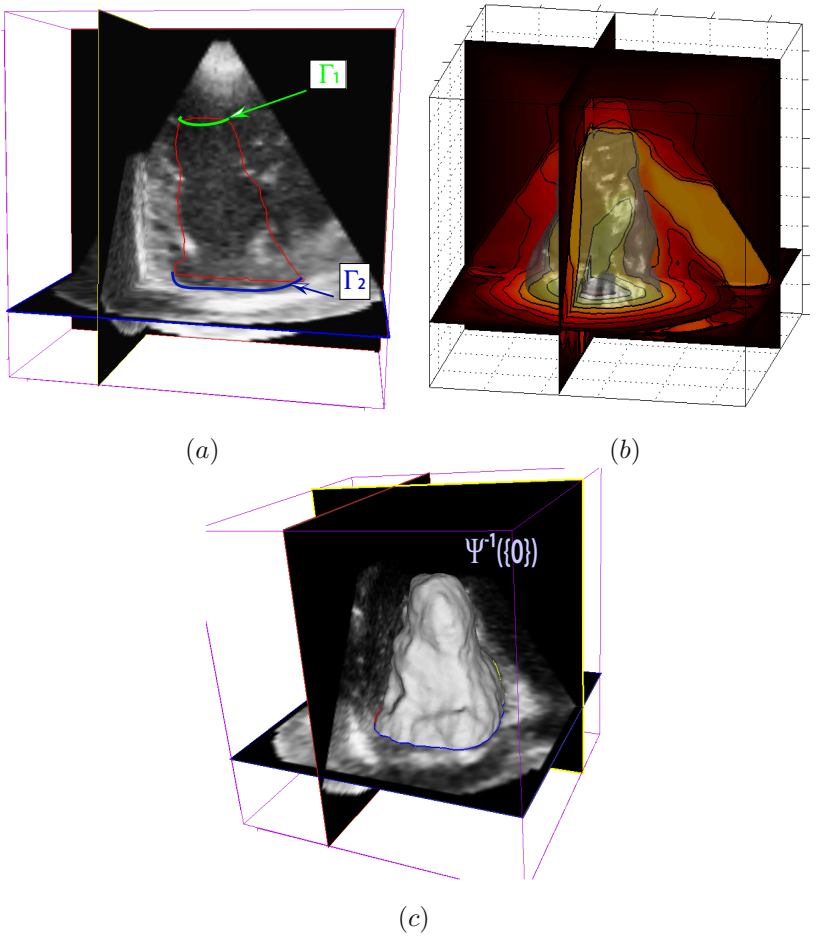

Fig. 6. (a) shows a plane of a 3D ultrasound volume obtained from a patient whose echogenicity is low. This image is difficult to segment. (b) shows some level sets of our solution Ψ and a volume representation of the zero level set. (c) displays the segmentation obtained with our method(see please the electronic color version).

256 we used a personal computer with a 1.4Ghz processor and 512 Mb of RAM. The segmentation is obtained in less than 15 seconds.

In our last example, shown in figure 6, we display the segmentation of a left ventricle. In this case the information given by the two constraining curves is crucially important, since the echogenicity of the patient generates a very low visibility.

6 Conclusion

In this paper we have presented a method that generalizes globally minimal paths for curve segmentation in 2D to surface segmentation in 3D. Our model is initialized by two user-supplied curves which we maximally exploit partly by the fact that the surface we generate is constrained to contain them. We have developed a novel implicit approach that, through a linear partial differential equation, exploits the solution to the Eikonal equation and generates a function whose zero level set contains all the globally minimal paths between the constraining curves. Hence, our approach is not prone to local minima traps as are other active surface approaches. It is especially well suited for medical image segmentation, in particular for ultrasound images segmentation. In cases where the image quality is very poor, our approach handles the introduction of additional information coming from the practitioner in a very natural manner: a few 2D segmentations can be enough to generate a coherent, complete surface.

References

1. L. Ambrosio. Transport equation and Cauchy problem for BV vector fields. *Preprints Scuola Normale Superiore, Department of Mathematics: http://cvgmt.sns.it/people/ambrosio/*, 2003.
2. R. Ardon and L.D. Cohen. Fast constrained surface extraction by minimal paths. *2nd IEEE Workshop on Variational, Geometric and Level Set Methods in Computer Vision*, pages 233–244, October 2003.
3. R. Ardon and L.D. Cohen. Fast Constrained Surface Extraction by Minimal Paths. *To appear in IJCV*, 2005.
4. F. Bouchut, F. James, and S. Mancini. Uniqueness and weak stability for multi-dimensional transport equations with one-sided lipschitz coefficient. *Prépublications du département Mathématiques et Applications, Physique Mathématique d'Orléans*, 2004.
5. A.M. Bruckstein. On shape from shading. *CVGIP*, 44(2):139–154, November 1988.
6. V. Caselles, R. Kimmel, and G. Sapiro. Geodesic active contours. *IJCV*, 22(1):61–79, 1997.
7. V. Caselles, R. Kimmel, G. Sapiro, and C. Sbert. Minimal-surfaces based object segmentation. *IEEE Transactions On Pattern Analysis and Machine Intelligence*, 19(4):394–398, April 1997.
8. L.D. Cohen. On active contour models and balloons. *CVGIP*, 53(2):211–218, 1991.
9. L.D. Cohen. Avoiding local minima for deformable curves in image analysis. In *Curves and Surfaces with Applications in CAGD*, Nashville, 1997. Vanderbilt Univ. Press.
10. L.D. Cohen and R. Kimmel. Global minimum for active contour models: A minimal path approach. *IJCV*, 24(1):57–78, August 1997.
11. W. P. Crowley. Numerical advection experiments. *Monthly Weather Review*, 96:1–11, 1968.
12. T. Deschamps and L.D. Cohen. Fast extraction of minimal paths in 3D images and applications to virtual endoscopy. *Medical Image Analysis*, 5(4), December 2001.

13. O. Gerard, T. Deschamps, M. Greff, and L. D. Cohen. Real-time interactive path extraction with on-the-fly adaptation of the external forces. *European Conference on Computer Vision*, june 2002.
14. C. Y. Kao, S. Osher, and J. Qian. Lax-Friedrichs sweeping scheme for static Hamilton-Jacobi equations. *Journal of Computational Physics*, 26:367–391, Mai 2004.
15. M. Kass, A. Witkin, and D. Terzopoulos. Snakes: Active contour models. *International Journal of Computer Vision*, 1(4):321–331, 1988.
16. P. D. Lax and B. Wendorff. Systems of conservation laws. *Communications on Pure and Applied mathematics*, 17:381–398, 1964.
17. R. J. LeVeque. High-resolution conservative algorithms for advection in incompressible flow. *SIAM Journal on Numerical Analysis*, 33(2):627–665, April 1996.
18. C. Mantegazza and A. C. G. Mennucci. Hamilton-Jacobi equations and distance functions on Riemannian manifolds. *Appl. Math. Opt.*, 47(1):1–25, 2003.
19. N. Paragios. *Geodesic Active Regions and Level Set Methods: Contributions and Applications in Artificial Vision*. PhD thesis, Université de Nice Sophia-Antipolis, France, 2000.
20. J.A. Sethian. A fast marching level set method for monotonically advancing fronts. *Proceedings of the National Academy of Sciences*, 93(4):1591–1595, February 1996.
21. J.A. Sethian. *Level set methods: Evolving Interfaces in Geometry, Fluid Mechanics, Computer Vision and Materials Sciences*. Cambridge University Press, University of California, Berkeley, 2nd edition, 1999.
22. P. K. Smolarkiewicz. The multi-dimensional crowley advection scheme. *Monthly Weather Review*, 110:1968–1983, 1982.
23. J. N. Tsitsiklis. Efficient algorithms for globally optimal trajectories. *IEEE Transactions on Automatic Control*, 40(9):1528–1538, September 1995.
24. A. Yezzi, S. Kichenassamy, A. Kumar, P. Olver, and A. Tannenbaum. A geometric snake model for segmentation of medical imagery. *IEEE Transactions On Medical Imaging*, 16(2):199–209, Avril 1997.
25. A. Yezzi and J. L. Prince. An Eulerian PDE Approach for Computing Tissue Thickness. *IEEE Transactions On Medical Imaging*, 22:1332–1339, October 2003.
26. A.L. Yuille, P.W. Hallinan, and D.S. Cohen. Feature extraction from faces using deformable templates. *International Journal of Computer Vision*, 8(2):99–111, August 1992.
27. S.C. Zhu and A. Yuille. Region competition: Unifying snakes, region growing, and bayes/mdl for multiband image segmentation. *IEEE Transactions On Pattern Analysis and Machine Intelligence*, 18(9):884–900, September 1996.